Published in IET Radar, Sonar and Navigation
Received on 13th January 2009
Revised on 17th March 2009
doi: 10.1049/iet-rsn.2009.0007

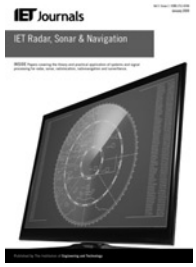

ISSN 1751-8784

New waveform design for magnetron-based marine radar

N. Levanon

Department of Electrical Engineering – Systems, Tel Aviv University, Chaim Levanon Street, Tel Aviv 69978, Israel
E-mail: nadav@eng.tau.ac.il

Abstract: At their long-range mode, conventional magnetron-based marine radar use low pulse repetition frequency (PRF) to extend the unambiguous range, and increase the pulse-width to regain the average power. The proposed new waveform maintains narrow pulses and high PRF even at the long-range mode. Range ambiguity is mitigated by periodic 'yes–no' coding of the transmitted pulse train. Using narrow pulses improves the range resolution and reduces the radial dimension of the illuminated clutter.

1 Introduction

Marine radar is one of the most common radar in use. It usually utilises a magnetron, allowing a low-cost product suitable for pleasure and fishing boats. The mode of operation of a typical marine radar (e.g. Furuno model 1715) changes with the range. For short range it typically uses narrow (80 ns) pulses and high (3000 pps) pulse repetition frequency (PRF). The typical values for long range are a pulse-width of 800 ns and a PRF of 600 Hz. The corresponding unambiguous ranges are 27 and 135 nm (nautical miles). The corresponding range resolutions are 12 and 120 m.

A main reason for decreasing the PRF in the long-range mode is to increase the unambiguous range. The main reason for increasing the pulse-width is to recover the average transmitted power (lost because of the lower PRF) and even increase it somewhat in order to raise the probability of detection of distant targets. In the numerical example given above, the average power in the long-range mode was doubled. Another way to increase the target reflected energy during the antenna dwell is to reduce the antenna rotation rate. In the case of the Furuno 1715, the rotation speed decreases from 41 rpm at the short-range mode to 24 rpm at the long-range mode.

The penalty of increasing the pulse-width is 2-fold: (a) the range resolution is degraded and (b) the radial dimension of the illuminated clutter increases. Since the cross-range (azimuth) dimension and the height dimension (relevant to precipitation clutter) also increase with the range, the clutter reflection volume that competes against the target reflection is greatly increased with the range.

In coherent radar, the narrow range resolution can be restored, without losing the reflected target energy, by using pulse compression. Magnetron-based radar does not have pulse compression capability. This paper shows how magnetron-based radar can maintain the narrow pulse-width and the high PRF in the long-range mode as well, while mitigating the short unambiguous range problem associated with high PRF.

2 Principle of operation

In non-coherent radar, mitigating the range ambiguity of high PRF can be implemented by on–off (or yes–no) inter-pulse coding of the original transmitted pulse train and correspondingly coding the reference pulses in the receiver. A simple example is described in Table 1. The pulse train is divided into groups of M (=10) pulses. Half of them are transmitted ('1' in row 2) and half are not ('0'). The reference sequence in the receiver, with which the detected return is cross-correlated, appears in row 3. Transmitting the ten pulse sequences continues repeatedly. It is required that at least three such sequences will be reflected from the target during the duration in which the rotating antenna beam illuminates the target (the dwell time).

Table 1 Transmitted and reference pulse coding

Pulse no.	1	2	3	4	5	6	7	8	9	10
trans.	0	1	1	0	0	1	0	1	0	1
ref.	−1	1	2	−2	−1	1	−1	1	−1	1

Table 1 shows that while two pulses (2 and 3) are still separated by the original pulse repetition interval (PRI), the average PRI doubled. Hence, to recover the number of pulses per unit time, the original PRF should be doubled (if the hardware allows).

Even with the original PRF (3000 in the case of Furuno 1715), the requirement of three sequences (30 original pulses) is easily met. The number of PRIs during the antenna dwell time is given by

$$N_{\text{dwell}} \simeq \frac{\text{PRF}\theta_{\text{H}}}{6\omega} \times \frac{3000 \times 5.2}{6 \times 24} = 108 \qquad (1)$$

where θ_{H} is the antenna horizontal beamwidth in degrees and ω is the antenna rotation rate in revolutions per minute. If the PRF could be doubled, 216 pulse positions per dwell will be available (about 21 sequences of 10 pulses) and the reference could contain several sequences of ten pulse positions. The number of integrated pulses is the number of pulses in the reference.

The envelope of five consecutive sequences of the 'yes–no' coded pulse train is shown in the top subplot of Fig. 1. The bottom subplot shows two reference sequences stored in the receiver. The delay scale is in units of the PRI ($= T_r$), with a periodicity of 10 (i.e. the sequence duration). The cross-correlation between the detected envelope of five transmitted pulse sequences and two reference sequences is shown in Fig. 2. As long as the reference is completely overlapped by the signal, we obtain an ideal (free of positive sidelobes) periodic response, with a period that equals the sequence duration. For an original PRF of 3000 Hz the unambiguous range is 270 nm. If the original PRF is doubled (6000 Hz), the unambiguous range will become 135 nm.

3 Comparison

Table 2 compares the existing and suggested systems with respect to average power, unambiguous range and clutter illuminated area A_{clutter} at a range R of 20 km, where

$$A_{\text{clutter}} = \frac{1}{2} C t_{\text{p}} R \theta_{\text{H}} \qquad (2)$$

Here C is the velocity of propagation and t_{p} is the pulse-width. Comparing the existing system with the suggested system, we note identical unambiguous range, but an order of magnitude reduction (i.e. improvement) of the illuminated clutter area.

Another design parameter is the number of periods (in the conventional system) or sequences (in the proposed system) that should be integrated, which means the number of reference periods (or sequences) with which the detected envelope of the received signal is cross correlated. In order not to widen the azimuth resolution beyond what the antenna horizontal beamwidth determines, the duration of the reference should not be longer than about 40% of the dwell time. From Table 2 we conclude that in the

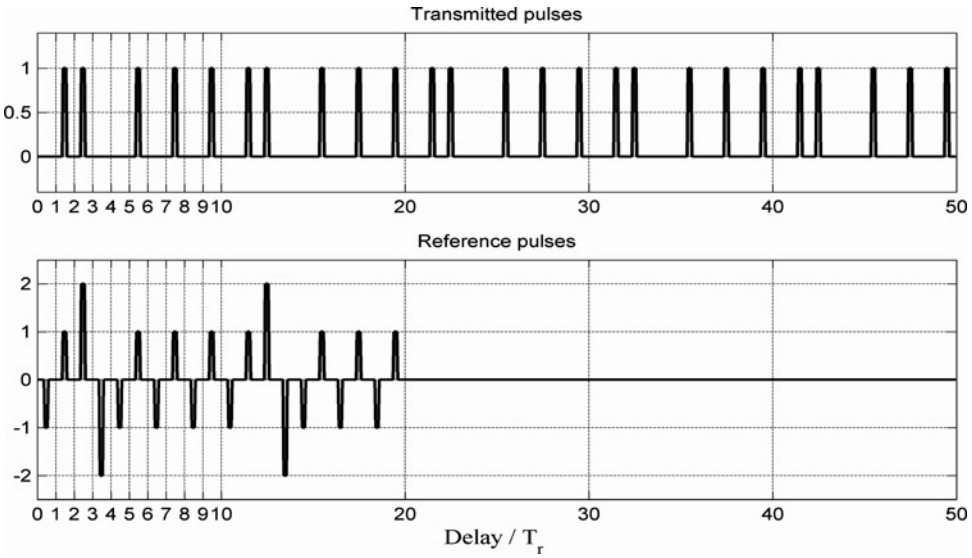

Figure 1 *Five consecutive sequences of the 'yes–no' coded pulse train (top) and two reference sequences (bottom)*

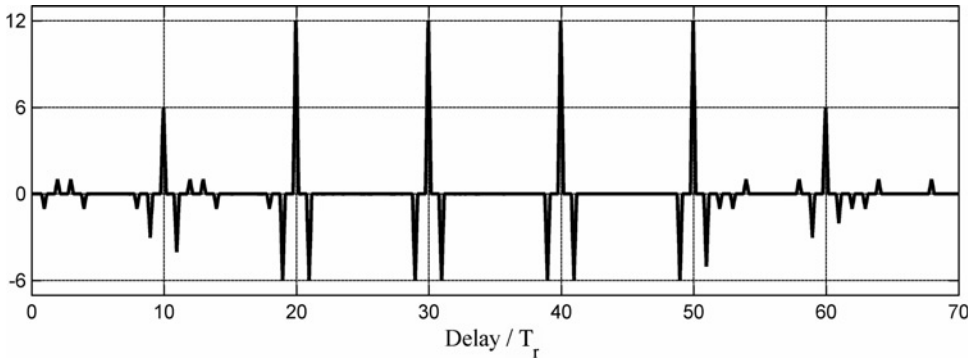

Figure 2 *Cross-correlation between five transmitted pulse sequences and two reference sequences*

Table 2 Parameters of existing and proposed systems

Parameter	Present system	Suggested system
pulse-width [μs]	0.8	0.08
PRF	600	6000
% of pulses transmitted	100%	50%
average transmitted power, [W], (assuming 2.2 kW peak)	1.0	0.5
dwell time, [s] (assuming 24 rpm, 5.2° beamwidth)	0.0361	0.0361
number of PRI per dwell	21.6	216
number of sequence repetitions (sequence = 10 PRI's) per dwell	—	21.6
unambiguous range	250 km, 135 nm	250 km, 135 nm
clutter illuminated area at a range of 20 km	220 000 m^2	22 000 m^2

conventional system about eight pulses should be integrated, and in the proposed system the reference should include about ten sequences, namely 50 pulses.

4 Simulations using Hamming weighted reference (without noise, clutter and target fluctuations)

The sidelobe-free periodic response assumes constant amplitude received pulses. However, the antenna pattern amplitude modulates the reflected pulses, which raises the question of how well the sidelobe-free periodic response is preserved. In order to isolate and study that particular problem we performed simulation without noise, clutter and fluctuations. The simplified radar scene involves two non-fluctuating targets – target 1 (20 km at 10°) and target 2 (35 km at 25°) of equal received reflection. The two-way antenna gain pattern was arbitrarily chosen as

$$g(\theta) = \left(\frac{\sin\alpha}{\alpha}\right)^2, \quad \alpha = \frac{\theta\sqrt{3}}{2\theta_{3\,\mathrm{dB}}} \tag{3}$$

In order to reduce the computation load some signal parameters were modified compared to Table 2 and are shown in Table 3. Particularly exaggerated are the pulse-widths. Each is about five times the width that will be used in reality. The PRF of the proposed system was increased to 10 kHz, yielding a unambiguous range of 150 km. (Without the 'yes/no' coding it would have been 15 km.) The 0.167 μs interval between samples of the received signal equals 1/3 the width of the 0.5 μs pulse, used in the simulation.

Table 3 Parameters used in simulations

Parameter	Conventional system	Suggested system
pulse-width, [μs]	5.0	0.5
PRF	500	10 000
% of pulses transmitted	100%	50%
sampling interval, [μs]	0.167	0.167
number of PRI's integrated	8	—
number of sequences integrated (a sequence = 10 PRI's)	—	12

doi: 10.1049/iet-rsn.2009.0007

Our simulations revealed that if the reference signal, which contains 12 sequences, is uniformly weighted, the delay response exhibits range sidelobes of −35 dB, whereas Hamming amplitude weighting restored a near ideal sidelobe-free periodic range response. The output of the processed reflected signal (proposed system, with Hamming weighted reference) is shown in Fig. 3. The processed reception of an attenuated, un-delayed copy of the transmitted signal, labelled 'direct signal', is also plotted and serves as a reference for zero delay. The top subplot contains the output from both targets (#1 on the left). The bottom subplot zooms on one sequence period of a processed reflection from target 1. We emphasise again that there are 10 PRIs between repetitions of the processed target response, and in five out of those 10 PRIs pulses were transmitted.

Using logarithmic vertical scale (Fig. 4), it is possible to also see the sidelobes of the delay response caused by the non-uniform amplitude of the received returns. The horizontal axis of Fig. 4 (as well as of Figs. 9, 10, 14 and 15) is time in units of the sample number. Thanks to the Hamming weighting the sidelobes (around samples 4×10^5 and 10×10^5) are lower than −50 dB. The Hamming weighted reference pulses are shown in Fig. 5. A brute-force (and not necessarily efficient) implementation of a processor with the weighted reference is through a very long finite impulse response (FIR) filter. The number of elements should be equal to the number of samples within the duration of the 12 sequences in Fig. 5. Only a small fraction of the FIR coefficients, those corresponding to the 120 pulse locations, will be non-zero. Their values will be those plotted in Fig. 5. Note that in the case of uniform weighting, the FIR coefficients will use only five values (0, ±1, ±2).

The expected radar screen in the proposed system (using Hamming weight) is shown in Fig. 6. Fig. 7 is a zoom on target 1. The corresponding zoom on target 1, of the conventional system (using uniform weighting), appears in Fig. 8. The considerable spread in the radial direction was caused by ten times wider pulse-width.

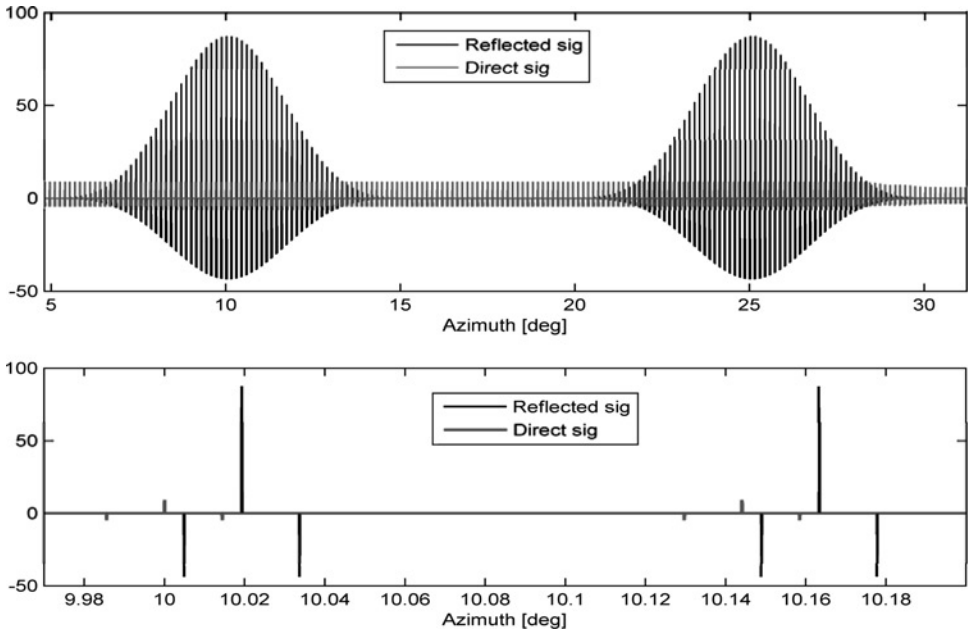

Figure 3 *Proposed system processed reflected signal and processed direct signal*

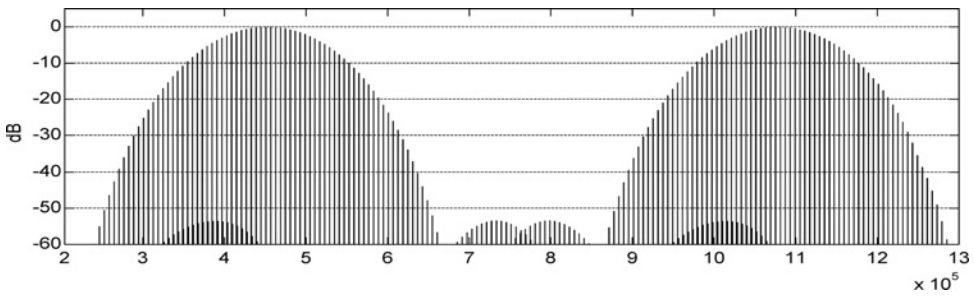

Figure 4 *Proposed system processed reflected signal using log scale to accentuate range sidelobes*
Horizontal scale in sample units (interval between samples = 0.167 μs)

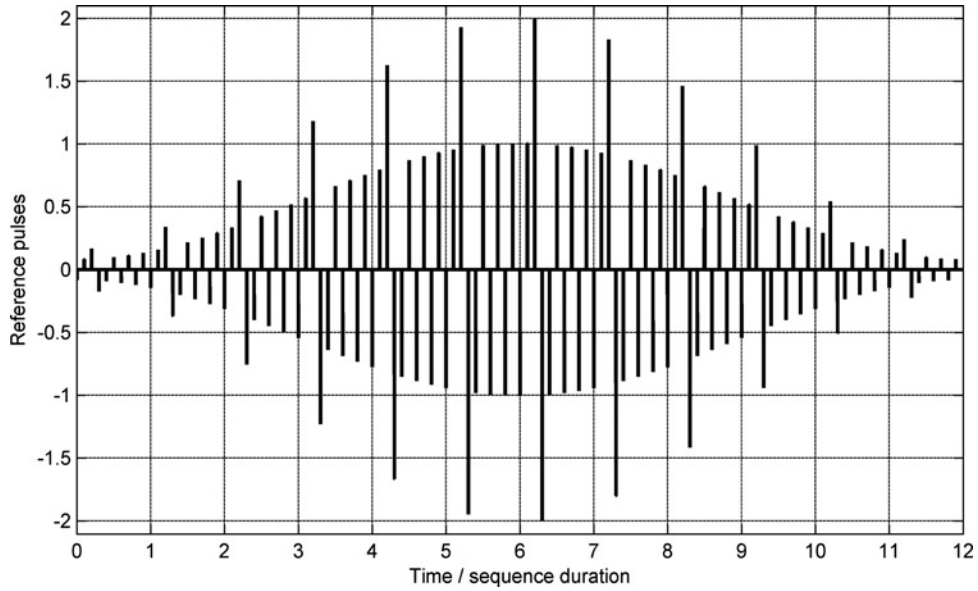

Figure 5 *Hamming weighted reference pulses*

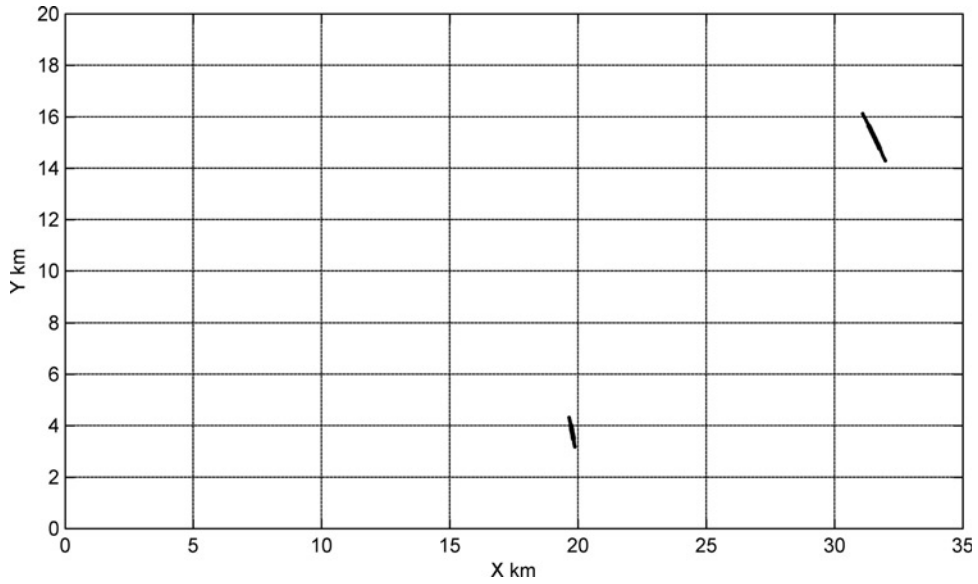

Figure 6 *Expected radar display of the proposed system*

5 Simulations (with noise) and signal-to-noise ratio loss considerations

An interesting by-product of the proposed signal and its processor is a very meaningful change in the probability density function (PDF) of the output because of noise. It stems from the fact that the reference sequence (see Table 1) contains equal positive and negative values. With noise-only input, the output of a square-law envelope detector multiplied by the zero-average reference sequence will exhibit zero mean and a near Gaussian PDF [1].

The corresponding output, y, because of noise only, in a conventional integrator of M samples (following square-law envelope detector) will have the well known PDF

$$p(y) = \frac{1}{2\beta^2(M-1)!}\left(\frac{y}{2\beta^2}\right)^{M-1}\exp\left(\frac{-y}{2\beta^2}\right) \simeq \frac{1}{2\beta^2}\left[\frac{y-e}{(M-1)2\beta^2}\right]^{M-1}\exp\left(\frac{-y}{2\beta^2}\right) \quad (4)$$

where β is the root mean square value of a noise sample.

The two different noise PDFs are clearly evident when the simulations include narrow-band noise. Output samples of

IET Radar Sonar Navig., 2009, Vol. 3, Iss. 5, pp. 530–540
doi: 10.1049/iet-rsn.2009.0007

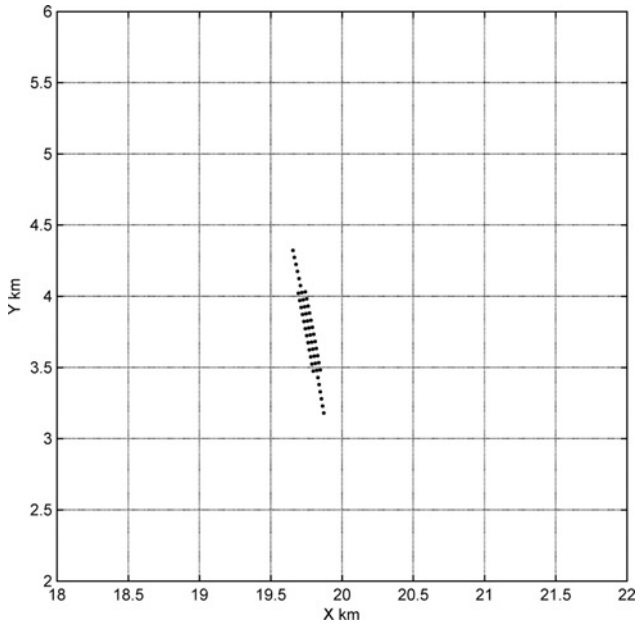

Figure 7 *Zoom on target 1 (proposed system)*

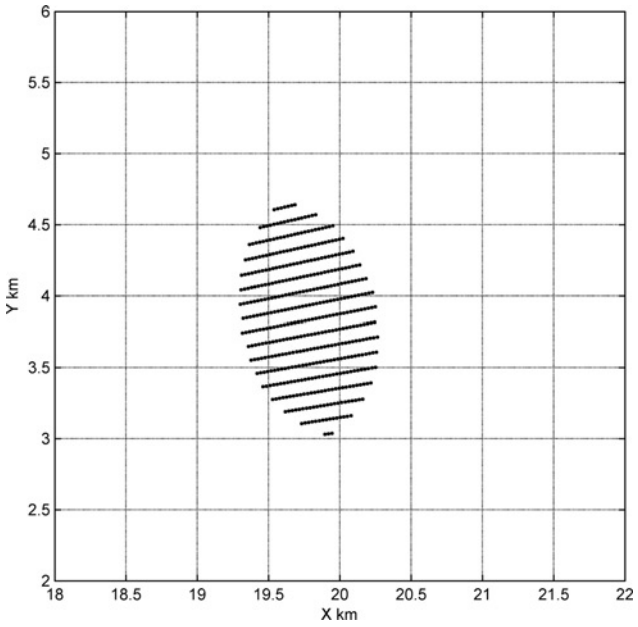

Figure 8 *Zoom on target 1 (conventional system)*

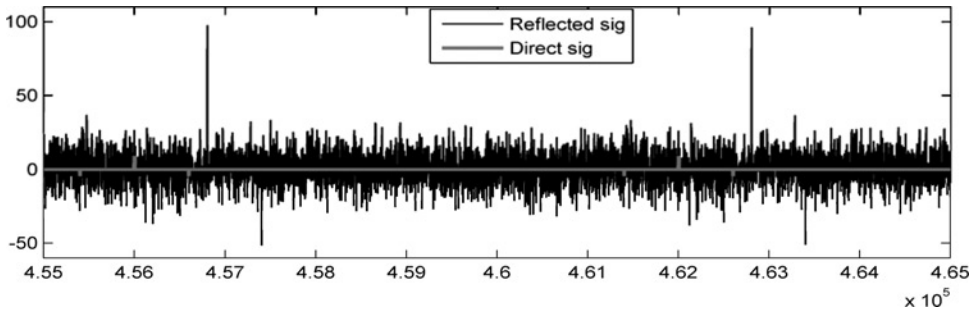

Figure 9 *Processed reflected signal with noise (proposed system)*
Linear vertical scale

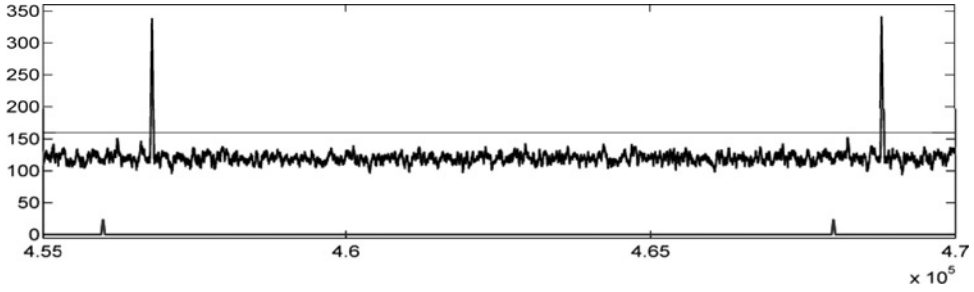

Figure 10 *Processed reflected signal with noise (conventional system)*
Linear vertical scale

the two systems are given in Figs. 9 and 10. Note that the threshold stage will use only the one-way rectified output (positive values) of Fig. 9.

PDFs of the outputs of the proposed waveform with Hamming weighted reference (Fig. 11), without weighting (Fig. 12) and of an un-weighted video integration of $M = 60$ pulses (Fig. 13), were obtained using 20 000 Monte-Carlo runs. The thresholds in each one of the three simulations were set to achieve a probability of false alarm of $P_{FA} = 0.001$. The single-pulse SNR was set to achieve a probability of detection of $P_D = 0.95$. The results are summarised in Table 4.

Intuition may have suggested that the proposed system will exhibit about 3 dB SNR loss, because the number of reference pulses (120) is twice the number of transmitted

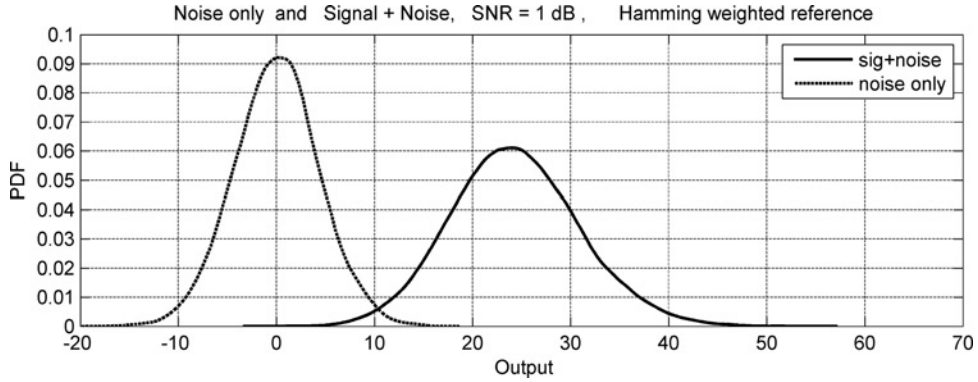

Figure 11 *PDF of the output of the proposed waveform (60 pulses) with Hamming weighted reference*

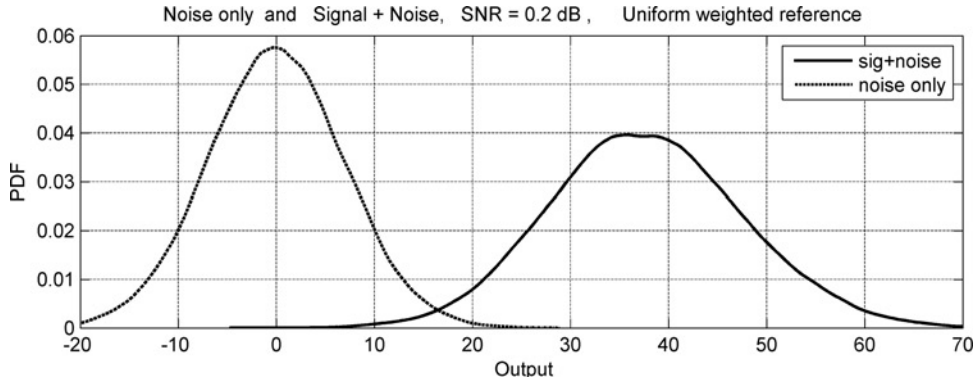

Figure 12 *PDF of the output of the proposed waveform (60 pulses) with uniform weighted reference*

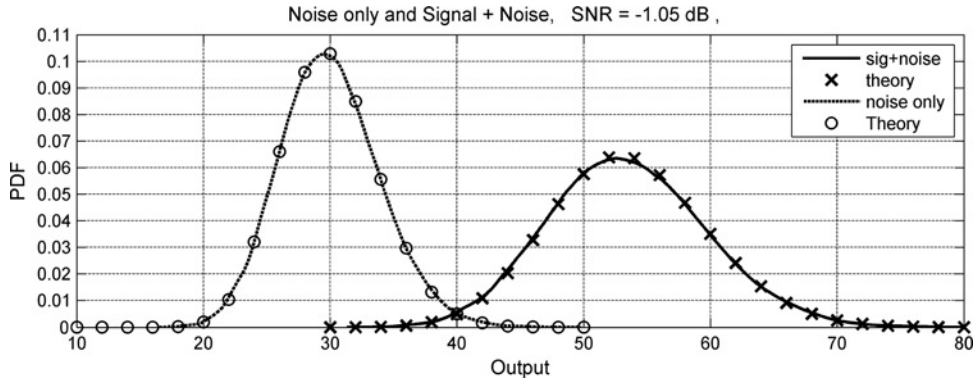

Figure 13 *PDF of the output of non-coherent integration of 60 non-fluctuating pulses, following square-law envelope detection*

pulses (60). However, the detection simulations indicate only 1.25 dB loss. This is due to the fact that the noise received during 60 reference pulses is subtracted from the noise received during the other 60 reference pulses. The additional SNR loss caused by using Hamming weighted reference pulses is only 0.8 dB.

Clutter is another important limiting factor of the detection range. Figs. 7 and 8 show how a point target is spread in both systems. The spread also shows the area above which precipitation clutter returns accumulate. (At shorter ranges – also the area of the surface clutter itself.) So even without quantitative analysis or simulations we can predict that the clutter return will be proportional to the pulse-width. Since the pulse-width in the proposed system is going to be approximately one-tenth that of the conventional system, the reflection from clutter is expected to be about 10 dB lower.

doi: 10.1049/iet-rsn.2009.0007

Table 4 Parameters and relative SNR loss in the three simulations ($P_{FA} = 0.001$, $P_D = 0.95$)

	PDFs plotted in	Threshold level setting for $P_{FA} = 0.001$	Single pulse SNR, [dB] for $P_D = 0.95$	Relative SNR loss, [dB]
conventional video integration of 60 non-fluctuating pulses	Fig. 13	43.6	−1.05	0
the proposed waveform (60 transmitted pulses), un-weighted reference	Fig. 12	21.9	0.2	1.25
the proposed waveform (60 transmitted pulses), Hamming weighted reference	Fig. 11	14	1.0	2.05

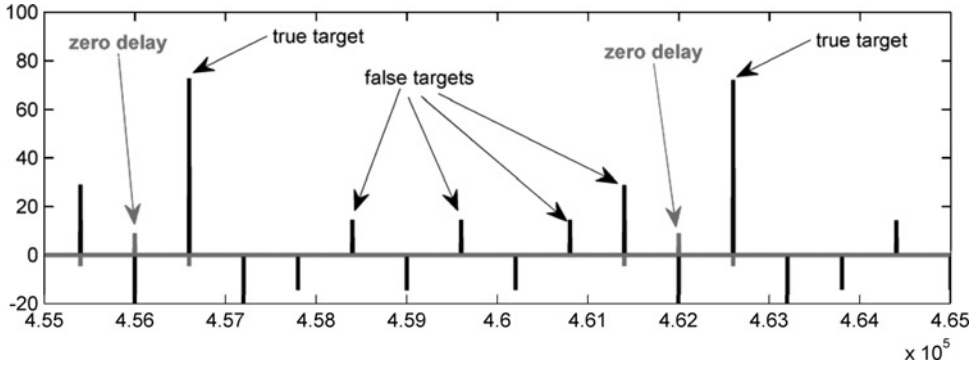

Figure 14 *Processor output with a partially blinded true target at 15 km (first false target at 60 km)*

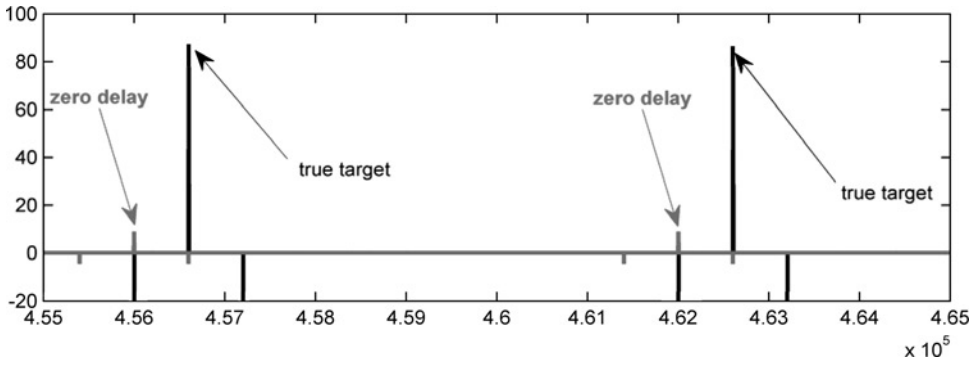

Figure 15 *The same delay span of processor output as in Fig. 11, when the target moved to 15 075 m*

6 Partial blind ranges

The 'yes/no' keying extended the unambiguous delay to ten times the PRI. This major advantage brings with it the minor problem of blind ranges, well known in high PRF radar. When all pulses are equally spaced by a fixed PRI, blanking the receiver during pulse transmission causes blind delays corresponding to multiples of the PRI. Luckily, the proposed waveform will suffer only partial blinding. Note from Table 1 that only one out of the five pulses is followed by a second pulse at a single basic PRI. Hence, when the PRF is 10 000, returns from targets at a range of 15 km will be blanked only for one out of the five pulses in each sequence. That means that the intensity of the integrated return from a target at 15 km will be 80% of a return from an identical target at 14.9 or 15.1 km. Measured intensities of targets at the next two blind ranges (30 and 45 km) will be reduced by 50%. These results were confirmed by simulations and some are shown in Figs. 14 and 15. The simulations also indicated that a target at the first 'partially blind' range of 15 km will produce weak false targets, the closest of which is at 60 km (intensities of 17%). A target at the second 'partially blind' range of 30 km will not result false targets. A target at the third 'partially blind' range of 45 km will result a false target at 135 km (intensity of 50%). The significance of the partial blinding is further reduced by the fact that the pulses are inherently

narrow, hence the receiver's 'off' durations are short. The expected range width of the partial blindness is similar to the minimum range (30 m in the Furuno 1715 radar). Obviously as the target moves away from the centre of the 'partially blind' 30 m swath its intensity increases, whereas the intensity of the false targets drops accordingly. The processor's periodic output as a function of delay, when the target is at the centre of the partially blind swath of 15 000 m, is plotted in Fig. 14. The output over the same delay span, when the target is at 15075 m, namely outside the partially blind swath, appears in Fig. 15. Comparing the two drawings demonstrates that the true target, when at the partially blind range, is attenuated (to 80%) but not blanked. In Fig. 14 the false target are also seen (the first one at 60 km).

The discussion above showed that the inherent advantage of partial visibility of targets located at blind ranges comes with a penalty. The penalty is the appearance of false targets starting at the fourth blind range, if there is a true target or strong clutter at the first blind range. If this penalty is unacceptable then both the advantage and the penalty can be removed by blanking the receiver at all 10 multiples of the basic PRI, and not only at the five multiples in which pulses were actually transmitted.

7 Target fluctuations and clutter

It requires a major project to study the behaviour and performances of the proposed waveform when the target fluctuates and is surrounded by clutter. The best conclusions are likely to come not from theory or simulations but from trials at sea. Qualitatively we should expect no serious degradation if the target fluctuations are scan-to-scan. To get some idea about what happens when the target fluctuations are pulse-to-pulse (worst case) and when there are clutter returns at the neighbouring range cells, we performed a simple simulation described in the Appendix. Note that pulse-to-pulse fluctuations can also be caused within the transmitter itself, although not as severely as those caused by a fluctuating target.

8 More waveforms

The ten element coding sequence (Table 1), used in the simulations, is only one of many possible sequences. The ten elements on–off code was based on Manchester-coded Ipatov 5 binary sequence [2, 3 (Section 6.5)]. The next Ipatov binary code is of length 13, which will become a 26 element on–off code after Manchester coding (Table 5). Peer [4] in his MSc thesis shows how to find periodic on–off codes for any length. However, their respective reference sequence, which will result in an ideal periodic cross-correlation, requires richer alphabet than Ipatov-based codes. An example of an 'on–off' code of length 14 is listed in Table 6. Note the irregular negative reference corresponding to pulse position no. 12. It hints to somewhat larger SNR loss than in codes based on Ipatov sequences.

Table 5 Twenty-six elements code

Pulse no.	Trans.	Ref.
1	1	2
2	0	−2
3	0	−3
4	1	3
5	0	−3
6	1	3
7	1	2
8	0	−2
9	0	−3
10	1	3
11	1	2
12	0	−2
13	1	2
14	0	−2
15	1	2
16	0	−2
17	1	2
18	0	−2
19	1	2
20	0	−2
21	0	−3
22	1	3
23	1	2
24	0	−2
25	1	2
26	0	−2

Table 6 Fourteen elements code

Pulse no.	1	2	3	4	5	6	7	8	9	10	11	12	13	14
trans.	0	1	0	0	1	0	0	1	1	1	0	1	0	1
ref.	−5	5	−2	−4	7	−4	−5	5	1	2	−2	−1	−2	5

doi: 10.1049/iet-rsn.2009.0007

9 Discussion and conclusions

The proposed marine radar waveform maintains the average power of a conventional marine radar waveform by using higher PRF and narrower pulses. The range ambiguity associated with high PRF is mitigated by inter-pulse periodic coding (yes/no). A main advantage is the much lower clutter illumination and the related improved range resolution. We also showed that opening the receiver twice as many times as there are pulses did not cause too high SNR loss. The relative loss compared to conventional video integration was 1.25 dB with un-weighted reference and 2.05 dB with Hamming weighted reference. Being able to keep using high-power magnetrons far outweighs such a loss. A drawback of high PRF systems – blind ranges, turns out to be only partial blindness and even that only over narrow range slots. There are still other drawbacks to the proposed system. For example, the system does not lend itself to simple sensitivity time control (STC). STC is traditionally used to reduce the receiver gain at close ranges where clutter echoes are relatively large. Another drawback is the need for a more sophisticated receiver processing. Still, most of the processing follows an envelope detector; hence phase information and complex numbers are not required. Another concern is some performances degradation if the target exhibits pulse-to-pulse fluctuations (e.g. Swerling models 2 and 4). Such a concern can be resolved best in sea trials, which hopefully will happen.

10 References

[1] PEER U., LEVANON N.: 'Compression waveforms for non-coherent radar'. IEEE Radar Conf., Boston, MA, USA, 17–20 April 2007

[2] IPATOV V.P., FEDOROV B.V.: 'Regular binary sequences with small losses in suppressing sidelobes', *Radioelectron. A. Commun. Syst. (Radioelektronica)*, 1984, **27**, (3), pp. 29–33

[3] LEVANON N., MOZESON E.: 'Radar signals' (Wiley, Hoboken, NJ, 2004)

[4] PEER U.: 'Pulse compression for non-coherent radar systems'. MSc thesis, Tel Aviv University, Faculty of Engineering, August 2007

11 Appendix: simulations with clutter and pulse-to-pulse fluctuations

In this simplified simulation a long periodic train of sequences according to Table 1 was transmitted. The reference was

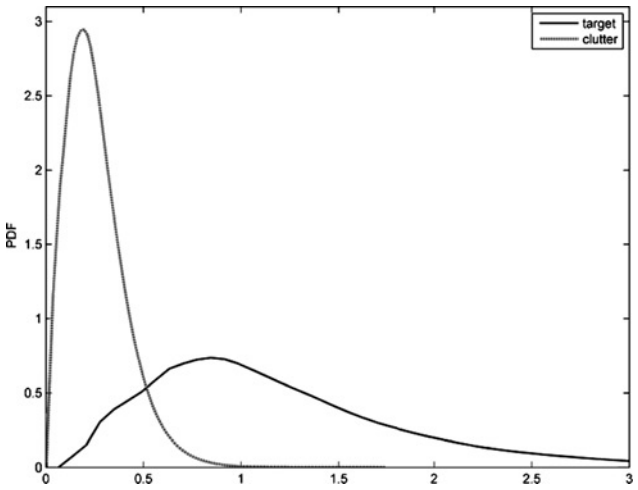

Figure 17 *PDF of target fluctuations and clutter*

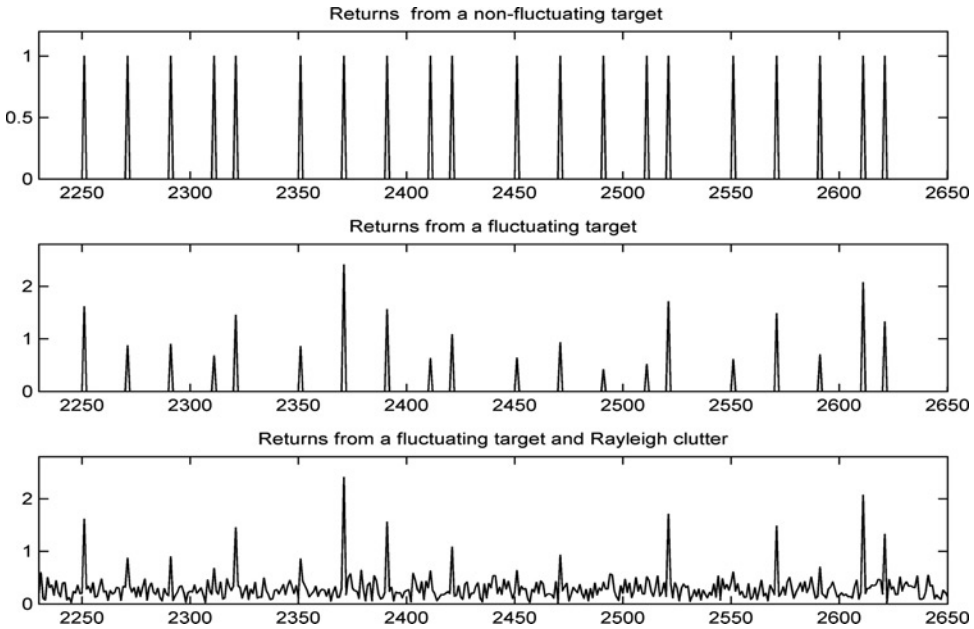

Figure 16 *Reflected returns from three different target and clutter models*

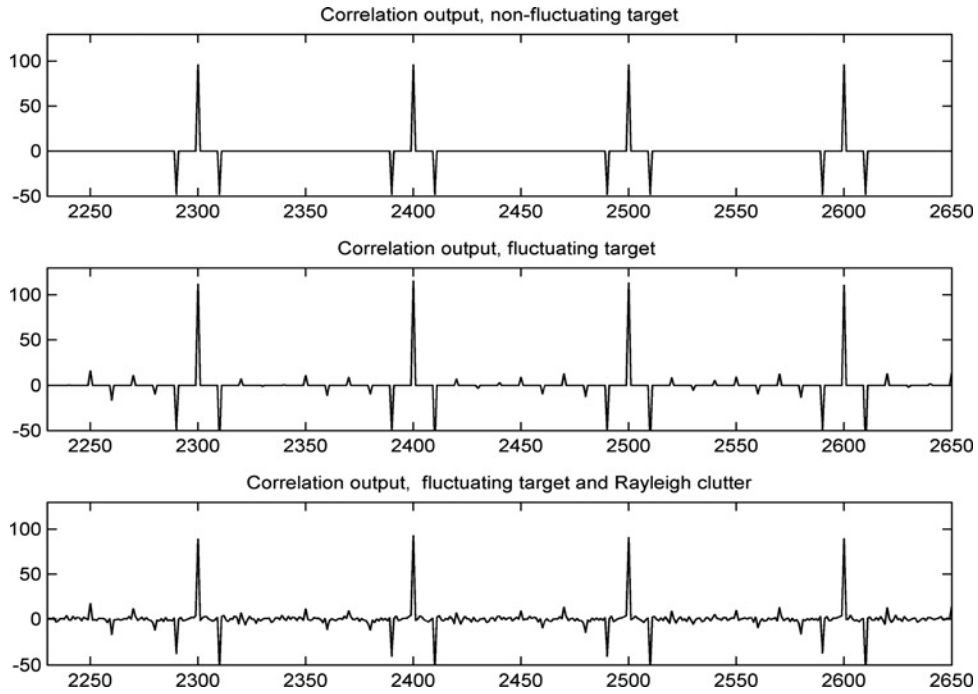

Figure 18 *Correlation outputs*

constructed from 16 consecutive reference sequences. Three different noise-free received reflections were used as plotted in Fig. 16: clutter-free reflection from a non-fluctuating target (top subplot); clutter-free reflection from a fluctuating target (middle); reflection from a fluctuating target plus Rayleigh clutter at all range cells (bottom). The target fluctuations were assumed uncorrelated from pulse-to-pulse, which is a worst-case situation for the proposed waveform. The vertical scales in Figs. 16 and 18 are intensities (linear) and the horizontal scales are delay.

The PDF of the target fluctuations and of the clutter appear in Fig. 17. The result of cross correlating the three received signals (shown in Fig. 16) with the 16 sequence reference signal are plotted in Fig. 18. Clearly, in the case of the non-fluctuating target the response of the correlator processor is ideal with no range sidelobes (top subplot). Despite severe pulse-to-pulse target fluctuations, the middle subplot shows only minor delay sidelobes. The relatively strong clutter affects the output (bottom subplot) in two ways: lower periodic mainlobes and more pronounced sidelobes. Still the signal-to-clutter ratio, seen in the bottom subplot of Fig. 18, suggests considerable margin for threshold setting that will yield low false alarm rate and high probability of detection.

doi: 10.1049/iet-rsn.2009.0007